

Surface Roughness-Hydrophobicity Coupling in Microchannel and Nanochannel Flows

M. Sbragaglia,¹ R. Benzi,² L. Biferale,² S. Succi,³ and F. Toschi^{3,4}

¹*Department of Applied Physics, University of Twente, P.O. Box 217, 7500 AE Enschede, The Netherlands*

²*Dipartimento Fisica and INFN, Università di Tor Vergata 00133 Roma, Italy*

³*Istituto per le Applicazioni del Calcolo CNR, Viale del Policlinico 137, 00161 Roma, Italy*

⁴*INFN, Sezione di Ferrara, via G. Saragat 1, I-44100, Ferrara, Italy*

(Received 18 April 2006; published 17 November 2006)

An approach based on a lattice version of the Boltzmann kinetic equation for describing multiphase flows in nano- and microcorrugated devices is proposed. We specialize it to describe the wetting-dewetting transition of fluids in the presence of nanoscopic grooves etched on the boundaries. This approach permits us to retain the essential supramolecular details of fluid-solid interactions without surrendering—actually boosting—the computational efficiency of continuum methods. The method is used to analyze the importance of conspiring effects between hydrophobicity and roughness on the global mass flow rate of the microchannel. In particular we show that smart surfaces can be tailored to yield very different mass throughput by changing the bulk pressure. The mesoscopic method is also validated quantitatively against the molecular dynamics results of [Cottin-Bizonne *et al.*, *Nat. Mater.* **2**, 237 (2003)].

DOI: [10.1103/PhysRevLett.97.204503](https://doi.org/10.1103/PhysRevLett.97.204503)

PACS numbers: 47.11.-j, 47.61.-k, 68.03.Cd, 83.50.Rp

The dynamics of microflows is crucially affected by the interaction of the fluid with the confining solid boundaries. Information on these interactions is usually conveyed into the formulation of proper boundary conditions for the fluid flow. Slippage properties have been reported in experiments and in molecular dynamics simulations, depending on the thermodynamical and wetting properties of the boundary (contact angle) and on the surface geometry [1–8]. A fundamental question arises as to whether the fluid really slips over the surface, or an apparent slip arises from surface inhomogeneities or complex interface with additional physics. It has been argued that a gas layer at the interface would alter the fluid dynamics in the bulk, leading to a mass flow rate increase even in the presence of pure no-slip [9–13]. This hypothesis is supported by the observation of nanobubbles trapped on the surface [14] and by a decreasing apparent slip length as the fluid is degassed [15].

The aim of this article is to discuss the complex effects, at the hydrodynamical scales, induced by the surface wetting properties in the presence of complex geometries in micro- and nanodevices. The results can be summarized in two main points. First, we provide neat evidence that the physics of the boundary conditions is quantitatively reproduced by modeling the fluid at mesoscopic level, by means of a minimal version of the Boltzmann equation, i.e., the lattice Boltzmann equation (LBE) [16,17]. This result is obtained by performing a quantitative comparison of “finite-volume” dewetting transitions against recent molecular dynamics simulations (MD) [1,18]. These supramolecular phenomena are indeed an ideal ground for mesoscopic kinetic methods. By supramolecular, we imply phenomena that do not depend on the specific details of the interaction potential, but only on some of its global properties, such as the ratio of potential to thermal energy

ϵ/kT , or surface tension/contact angle. Whenever these integral properties can be mapped one-to-one into the free parameters of the mesoscopic LB equation, the latter offers several orders of magnitude acceleration over atomistic methods. Far from being a mere technicality, this result opens the way to numerical investigations at spatial and time scales much larger than those currently available in most MD simulations. The time step of LB, thanks to its built-in conservation properties, can be of the order of the interaction time, while for MD it must be much shorter. Hence, even under the restrictive assumption of the same spatial resolution, LB would be about 2 orders of magnitude faster than MD. Further orders of magnitude are gained due to the fact that LB evolves a preaveraged distribution function, which does not need any averaging. The result is that LB is easily 3–4 orders of magnitude faster than MD, hence represents a method of choice for supramolecular microfluidics.

Second, we extend the MD results by investigating the critical dependency of the mass flow rate on the degree of roughness at constant bulk pressure. In particular we show that it is possible to combine geometry and hydrophobicity to design *smart surfaces*, with slippage properties that can be changed by a control parameter. The simplest LBE for unitary time lapse reads as follows [19]

$$f_i(\mathbf{x} + \mathbf{c}_i, t + 1) - f_i(\mathbf{x}, t) = \frac{1}{\tau} [f_i(\mathbf{x}, t) - f_i^{(\text{eq})}(\mathbf{x}, t)] + F_i, \quad (1)$$

where $f_i(\mathbf{x}, t)$ is the probability of finding a particle at site \mathbf{x} at time t , moving along the i th lattice direction defined by the discrete speeds \mathbf{c}_i with $i = 1, \dots, b$. The left-hand side of (1) stands for molecular free-streaming, whereas the right-hand side represents the time relaxation (due to collisional interactions) towards local a Maxwellian equilib-

rium. Finally, the term F_i represents a volumetric body force to be connected with bulk particle-particle interactions. In particular we will use a *mean field* term

$$F(\mathbf{x}, t) = \mathcal{G}_b \sum_i w_i \psi(\mathbf{x}, t) \psi(\mathbf{x} + \mathbf{c}_i, t) \mathbf{c}_i, \quad (2)$$

where $\psi(\mathbf{x})$ is a phenomenological pseudopotential (generalized density), $\psi(\mathbf{x}, t) = \psi[\rho(\mathbf{x}, t)]$, which depends on the local density, ρ , first introduced by Shan and Chen [20], w_i are normalization weights, and \mathcal{G}_b tunes the molecule-molecule interaction, i.e., it plays the role of the normalized *inverse temperature*, ϵ/KT , with ϵ the molecular energy scale and KT the thermal energy. Here we choose the standard form $\psi = \sqrt{\rho_0} \{1 - \exp(-\rho/\rho_0)\}$, with the reference density $\rho_0 = 1$, in lattice units. Note that this choice for large densities is saturating $\psi(\rho \gg \rho_0) \rightarrow \text{const}$, a requirement meant to mimic the *hard-core* repulsion of standard particle-particle potentials to prevent unphysical density accumulation. Other mesoscopic approaches for two-phase fluids can also be defined by using a free energy description of the surface physics [21,22].

In spite of its simplicity, the Shan-Chen approach provides two crucial ingredients of nonideal fluid behavior: a nonideal equation of state and a nonzero liquid-vapor surface tension, σ_{lv} . Both features are encoded in the expression of the nonideal momentum flux tensor whose bulk contribution $P_b = c_s^2 \rho + \frac{1}{2} c_s^2 \mathcal{G}_b \psi^2$, with c_s the sound speed velocity, is clearly dependent on the inverse temperature \mathcal{G}_b .

If we further assume that the density field $\rho(\mathbf{x})$ matches a given value ρ_w at the boundary, we can regard ρ_w as a free-parameter related to the strength of the fluid-solid interactions and use it to parametrize the *contact angle* [23]. Notwithstanding their inherently mesoscopic character, the parameters \mathcal{G}_b and ρ_w for the kinetic distributions used here carry no less physical content than their atomistic counterparts (inverse temperature and particle-wall interactions in MD simulations [8]). In order to study the wetting (dewetting) transition on micropatterned (nanopatterned) surfaces (see Fig. 1) we have integrated the LBE Eq. (1) in a 2D lattice using the nine-speed 2DQ9 model ($b = 9$), one of the most used 2D-LBE scheme, due to its superior stability [24,25]. We have used the two geometries described in Fig. 1. The first geometry is used to benchmark the method, the second to demonstrate the possibility to design a *smart surface* with slippage properties tunable with continuity at changing the bulk pressure. In all simulations Eqs. (1) and (2) have been numerically integrated with $\tau = 0.8$ and fixed inverse temperature, $\mathcal{G}_b = -6.0$ (the critical value being $\mathcal{G}_b^{(c)} = -4$). Concerning the velocity field, following [23], we set it to be zero at the boundary by using bounceback boundary conditions (see also [26] for different choices). The bulk pressure P_b then delivers the corresponding value of the

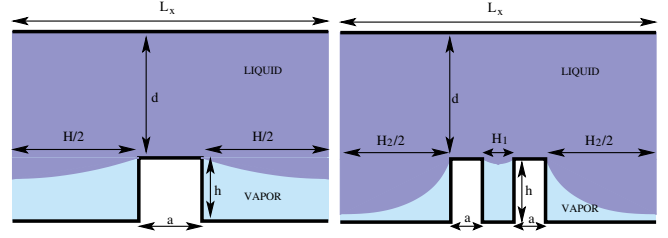


FIG. 1 (color online). Left: homogeneous roughness. A groove with depth $h = 33\Delta x$ and width $H = L_x - a$ (with $a = 10\Delta x$) is introduced on the bottom wall and periodic boundary conditions are assumed along x . In this configuration, the presence of vapor pockets inside the groove changes the “effective” boundary conditions felt by the bulk fluid, with a net decrease of drag when a pressure drop is applied. Right: channel with heterogeneous roughness. Two grooves of width $H_1 = 40\Delta x$ and $H_2 = 70\Delta x$ are present. The two grooves are filled separately at different values in the pressure and density diagram. The lattice spacing corresponds to $\Delta x \sim 0.3$ nm.

density ratio $\Delta\rho/\rho \sim 40$, while the surface tension is $\sigma_{lv} = 0.105 \pm 0.002$ in lattice units. The corresponding lattice spacing in physical units is obtained by matching the physical value of the liquid-vapor surface tension, with the one measured on the lattice, via the dimensional relation: $\sigma_{lv}^{\text{phys}} = KT/(\Delta x)^2 \sigma_{lv}$. For example, for water or vapor at $T = 540^\circ$ (there the density ratio is close to the values of our simulation) we have $\sigma_{lv}^{\text{phys}} = 0.022$ N/m, which yields $\Delta x \sim 0.3$ nm, a value which is comparable with the atomic range of the potentials used in MD. Molecular dynamics simulations have recently reported that the concerted effects of wetting phenomena and nanocorrugations can lead to a fairly substantial reduction of mechanical drag [1,18]. Specifically, the authors in [1,18] consider a nanometric channel flow with a regular sequence of longitudinal or transverse steps (with respect to the mean flow) along the solid wall of the channel, and show that, under suitable thermodynamic and geometric conditions, the presence of the steps triggers the formation of a gas film in the grooves within the obstacles. The liquid can then slide away over the gas film, thereby experiencing a significantly reduced mechanical drag. Such phenomenon may occur only at a critical pressure drop between the liquid and vapor phase, of the order of the capillary pressure, P_{cap} , given by the estimate [18]

$$P_{\text{cap}} = -\frac{2\sigma_{lv} \cos(\theta)}{L_x - a}. \quad (3)$$

In Fig. 2, we validate the LBE by a direct comparison with the MD results published in [1,18] with the same geometry and with comparable contact angle. As one can see, the agreement between LBE and MD is quantitative.

The plateaux for ΔP_{lv} in the range $0.9 < d/L_x < 1.05$ correspond to the pressure and density values at which the fluid is invading the corrugation, forming an interface

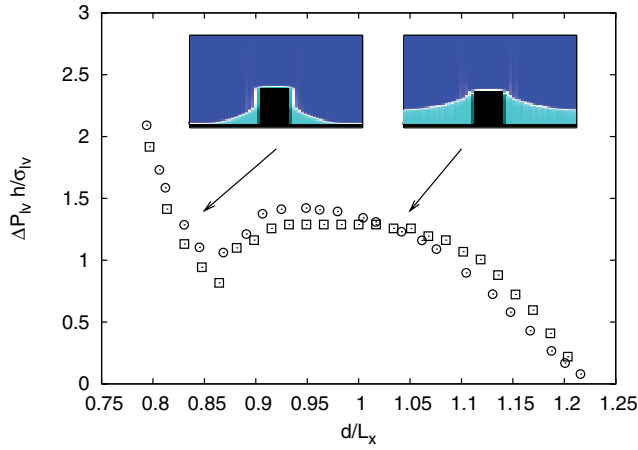


FIG. 2 (color online). The normalized pressure drop, $\Delta P_{IV} h/\sigma_{IV}$ between the two bulk phases, is shown as a function of the normalized distance d/L_x (see Fig. 1). LBE (\square) results have been obtained with a contact angle $\theta = 160^\circ$. MD results with the same contact angle are plotted with (\circ). The two insets represent the density configuration at the onset of the wetting/dewetting transition (right) and for a wetted configuration (left). The plateaux in the pressure curve defines the capillary pressure, P_{cap} .

which does not yet touch the bottom of the groove. This corresponds to the capillary pressure, P_{cap} . Reducing further d , i.e., increasing the average density, a change of concavity for $0.8 < d/L_x < 0.9$, is observed. This range corresponds to values when the interface starts to touch the bottom of the groove. The agreement of LBE with the capillary pressure (3) is checked in detail in Fig. 3, where we report the pressure changes for three different corrugations, $L_x - a$. In the inset of Fig. 3, we extract the value of

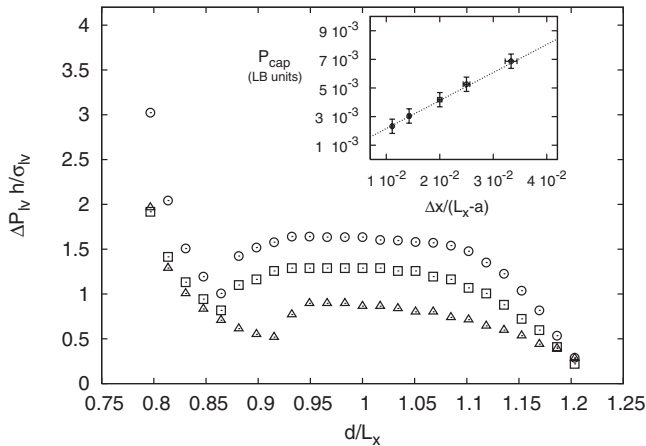


FIG. 3. Pressure variations at changing d for various roughnesses, $L_x = 50\Delta x$ (\triangle), $L_x = 60\Delta x$ (\square), $L_x = 80\Delta x$ (\circ), with $a = 10\Delta x$. In the inset, we show the relation (3). The slope is given by $2\sigma_{IV} \cos(\theta) = -0.196 \pm 0.006$ (LB units). With our surface tension $\sigma_{IV} = 0.105 \pm 0.002$ (LB units), this implies a best estimate of $\theta = 158^\circ \pm 6^\circ$.

$\sigma_{IV} \cos(\theta)$ from the slope of (3). The value of $\cos(\theta)$ is then obtained by estimating the surface tension, σ_{IV} , through Laplace's law for a droplet in equilibrium with its saturated vapor. The agreement of the contact angle measured in this way, $\theta = 158^\circ \pm 6^\circ$, with the analytical estimate, $\theta = 160^\circ$, obtained in [23] by imposing the mechanical equilibrium condition of the contact line is very satisfactory.

The comparison shown in Fig. 2 and 3 demonstrates the first result discussed in this Letter, namely, that the model introduced in [23] captures the correct interplay between roughness and wetting effects.

Even more complex behavior is observed for heterogeneous nanocorrugations, with the simplest case shown in the right panel of Fig. 1. In this case, one has two characteristic groove sizes, H_1 and H_2 , and hence two corresponding critical capillary pressures. The pressure-density diagram for this heterogeneous corrugation is shown in Fig. 4, where the two plateaux corresponding to the two capillary pressures coexist. This device may be considered a “smart” two-state surface, whose wetting properties and mass throughput (under the application of a pressure gradient) may be tuned by changing the bulk pressure. The dynamical response of the microchannel is investigated by applying a constant pressure gradient. In Fig. 5, we show the presence of a transition for a critical roughness where the mass flow rate starts to increase with respect to the perfect wetting situations reaching as much as 100% gain. The dynamical effects can be quantified in more detail by inspecting the momentum profile along the vertical direction without the vapor layer (fully-wetted configuration) and with a thin vapor layer starting to accumulate close to the bottom of the groove. This is shown in the inset of Fig. 5, where the *local* slip length is also depicted by extrapolation of the bulk profile inside the wall. As soon as a vapor layer is formed, the *local* slip length ramps-up,

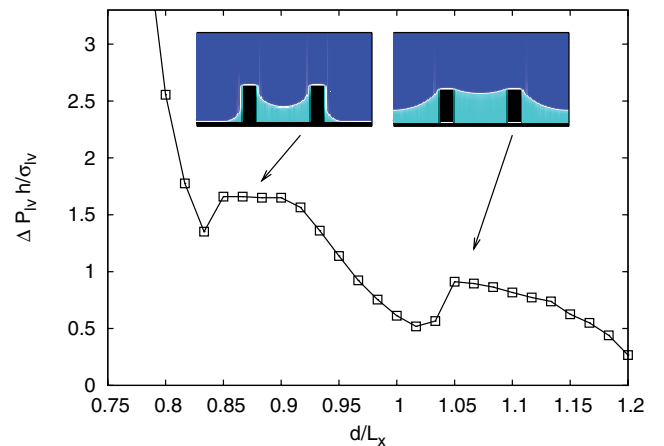


FIG. 4 (color online). Pressure variations for heterogeneous roughness (see right panel of Fig. 1). The two plateaux correspond to the case in which the liquid is starting to invade the widest groove (right) and when it is invading also the thinnest (left).

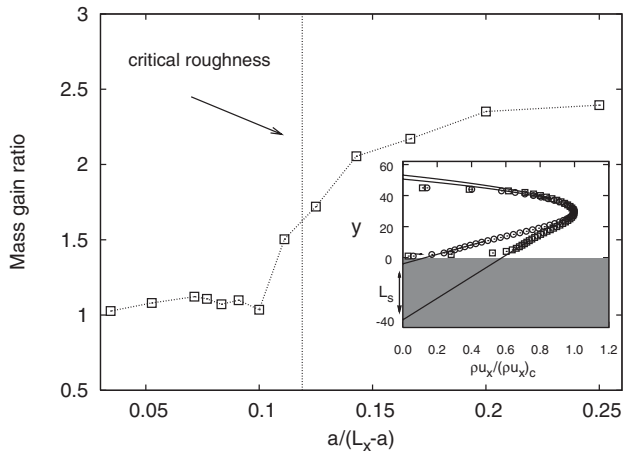


FIG. 5. Mass flow rate normalized to the fully-wetted case vs the effective roughness $a/(L_x - a)$. The bulk pressure is fixed to be $\Delta P_{lv} = 0.75\sigma_{lv}/h$. A critical roughness (vertical line) is given by the estimate of the capillary pressure, $0.75 \frac{a}{2h \cos(\theta)} = 0.119$ for $a = 10\Delta x$, $h = 33\Delta x$, $\theta = 158^\circ$. Inset: Momentum profile for a wetted (\circ), and almost dewetted configuration (\square). The geometry is the one of the left panel of Fig. 1 with parameters $h = 14\Delta x$, $a = 14\Delta x$, $L_y = 45\Delta x$, $L_x = 90\Delta x$. Both momentum profiles are shown for $x/L_x = 0.1$ and normalized with their center channel values. The straight lines correspond to extrapolations of the profiles inside the boundaries.

reaching values of the order of the channel height $45\Delta x \sim 15$ nm. Even larger values can be measured close to the dewetting transition, where a well-developed vapor layer is formed inside the groove (the so-called *superhydrophobic regime*).

Summarizing, we have shown that an extension of lattice Boltzmann equation for nonideal fluids, can *quantitatively* account for the concerted effects between wetting phenomena and geometrical irregularities. In particular, the presence of nano- or microirregularities in the flow geometries leads to sizeable effects with respect to the *infinite volume* liquid-gas transitions, as well as to a significant reduction of mechanical drag on the flowing fluid. The consequence of our results is twofold: from a theoretical perspective, it indicates that drag reduction via geometry-induced wetting transitions is a nonspecific phenomenon. On the practical side, the present LBE approach offers the opportunity to perform very efficient numerical simulations of complex micro- or nanofluidic phenomena at scales of direct experimental relevance, which are hardly accessible to atomistic simulations as, for example, the P - V diagram shown in Fig. 4. The most intriguing result is the possibility to design with a quantitative control new surfaces with ad hoc slippage properties. For example, it would be interesting to know the average slippage length in presence of fractal corrugation. Of course, many problems

remain open. From the theoretical point of view it is not known what is the correct continuum description of the lattice Boltzmann equations in presence of strong surface fluctuations. Also much more work is needed to make the mesoscopic model able to describe surface width over a larger range of scales.

Useful discussions with J.-L. Barrat, X. Shan, and S. Troian are kindly acknowledged. M.S. is grateful to STW (Nanoned programme) for financial support.

-
- [1] C. Cottin-Bizonne, J.-L. Barrat, L. Bocquet, and E. Charlaix, *Nat. Mater.* **2**, 237 (2003).
 - [2] E. Lauga, M.P. Brenner, and H.A. Stone, *Handbook of Experimental Fluid Dynamics* (Springer, New York, 2005).
 - [3] Y. Zhu and S. Granick, *Phys. Rev. Lett.* **88**, 106102 (2002).
 - [4] J. Ou and J.P. Rothstein, *Phys. Fluids* **17**, 103606 (2005).
 - [5] J.T. Cheng and N. Giordano *Phys. Rev. E* **65**, 031206 (2002).
 - [6] K. Watanabe and Y.H. Udagawa, *J. Fluid Mech.* **381**, 225 (1999).
 - [7] J. Baudry *et al.*, *Langmuir* **17**, 5232 (2001).
 - [8] L. Bocquet and J.-L. Barrat, *Phys. Rev. Lett.* **70**, 2726 (1993); P. Thompson and S. Troian, *Nature (London)* **389**, 360 (1997); N. V. Priezjev *et al.*, *Phys. Rev. E* **71**, 041608 (2005).
 - [9] E. Lauga and M.P. Brenner, *Phys. Rev. E* **70**, 026311 (2004).
 - [10] D.C. Trethewey and C.D. Meinhart, *Phys. Fluids* **16**, 1509 (2004).
 - [11] R. Benzi *et al.*, *Europhys. Lett.* **74**, 651 (2006).
 - [12] B. Li and D. Kwok, *Phys. Rev. Lett.* **90**, 124502 (2003).
 - [13] J. Harting *et al.*, *Europhys. Lett.* **75**, 328 (2006).
 - [14] J. W. G. Tyrrell and P. Attard, *Phys. Rev. Lett.* **87**, 176104 (2001).
 - [15] S. Granick *et al.*, *Nat. Mater.* **2**, 221 (2003).
 - [16] S. Chen and G. Doolen, *Annu. Rev. Fluid Mech.* **30**, 329 (1998).
 - [17] R. Benzi, S. Succi, and M. Vergassola, *Phys. Rep.* **222**, 145 (1992).
 - [18] C. Cottin-Bizonne *et al.*, *Eur. Phys. J. E* **15**, 427 (2004).
 - [19] P.L. Bhatnagar, E. Gross, and M. Krook, *Phys. Rev.* **94**, 511 (1954).
 - [20] X. Shan and H. Chen, *Phys. Rev. E* **47**, 1815 (1993); *Phys. Rev. E* **49**, 2941 (1994).
 - [21] M.R. Swift *et al.*, *Phys. Rev. E* **54**, 5041 (1996).
 - [22] A.J. Briant and J.M. Yeomans, *Phys. Rev. E* **69**, 031603 (2004).
 - [23] R. Benzi *et al.*, *Phys. Rev. E*, **74**, 021509 (2006).
 - [24] I. Karlin, A. Ferrante, and H.C. Oettinger *Europhys. Lett.* **47**, 182 (1999).
 - [25] B.M. Boghosian *et al.*, *Proc. R. Soc. A* **457**, 717 (2001).
 - [26] R. Benzi *et al.*, *J. Fluid Mech.* **548**, 257 (2006).